Numerical computation of the Rayleigh-Taylor instability for a viscous fluid with regularized interface properties

L. M. González-Gutiérrez[1] and A. de Andrea González[1,2]

[1]*School of Naval Engineering, Universidad Politécnica de Madrid, Avda. de la Memoria 4, 28040 Madrid, Spain*
[2]*Departamento de Física, Escuela Politécnica Superior, Universidad Carlos III de Madrid, Av. Universidad 30, 28911 Leganés, Spain*

In this article, the computation of the linear growth rates and eigenfunctions of the viscous version of the Rayleigh-Taylor instability by numerically solving the corresponding eigenvalue problem in the case of one-dimensional (1D) and two-dimensional (2D) geometries is studied. The 1D version is first validated in the particular inviscid case to be compared to the previous literature. The most unstable mode, also known as the first mode, which has the maximal linear growth rate has been extensively studied in previous literature. Higher modes have smaller eigenvalues, but the corresponding eigenfunctions present a more complex structure that contains multipeak shapes. In the extension to the 2D geometry, the length of the domain limits the wave number of the eigenvectors computed. In the extension to the 2D geometry the length of the domain limits the wave number of the eigenvectors computed. The importance of extending the results to the two-dimensional case is twofold. First, it opens up the possibility of generalizing the computation to more complex geometries that could contain fixed or floating objects and, second, allows the computation of flow instabilities in nonzero basic flows that could come from the steady Navier-Stokes solutions.

I. INTRODUCTION

The Rayleigh-Taylor instability (RTI), which occurs due to the gravitational instability of a heavy fluid overlying a lighter fluid [1], is important to a wide variety of applications: ferrofluids [2], tectonics [3], exploding foils [4], aerobreakup [5], and astrophysics [6,7].

Mikaelian [8] analyzed the Rayleigh-Taylor instability in two finite-thickness fluids including viscosity effects. A numerical dispersion relation was obtained for different thicknesses and Atwood numbers. He performed a one-dimensional (1D) analysis based on two fluids separated with a sharp interface using homogeneous Dirichlet and Neumann conditions for the velocity at the top and bottom boundaries and compatibility conditions at the interface. The 2D extension presented in this work allows the analysis of more complex flows and includes the possibility of studying diffuse interfaces, with the sharp interface just a particular case.

Obied Allah [9] investigated the finite-thickness effect of a slab of incompressible fluid with exponentially increasing density supported by a fluid of constant density in the presence of surface tension. He found that the finite thickness has a stabilizing effect on the RTI.

Morgan *et al.* [10] studied the behavior of the most unstable VRTI mode initiated with a diffuse interface. The results exhibit good agreement with the dynamic diffusion model of Duff *et al.* [11] for small wave numbers but produces larger growth rates for large wave-number perturbations.

Yu *et al.* [12] investigated the inviscid RTI for a fluid of tangent hyperbolic density. They obtained the multiple eigenvalues for the growth rates of the RTI and the corresponding eigenfunctions which may have potential applications in comprehending the mixing behavior existing in many areas. Moreover, they obtained a fitting expression for those eigenmodes in the dimensionless form, which agrees well with the numerical results for limited Atwood numbers $A_\rho \leqslant 0.8$. Dong *et al.* [13] revisited the physical problem that was studied in Ref. [12] by developing a short-wavelength asymptotic solution. Based on Wentzel-Kramers-Brillouin approximation, the growth rates of the RTI modes were obtained for Atwood numbers close to unity.

However, to the best of our knowledge no numerical study on the eigenvalue problem associated to the VRTI with a diffuse interface has been performed. Therefore, in this paper we carry out this research study in the case of 1D and 2D geometries based on a hyperbolic tangent distribution density profile that allows us to skip the compatibility conditions when sharp interfaces are simulated. Two-dimensional computation allows the possibility of studying more complex geometries and baseflows than the ones normally studied in the RTI; consequently, the interface instability of a wade variety of hydrodynamic problems can be studied.

II. PROBLEM SETUP

The strategies to perform the linear stability analysis are presented in this section. To study the viscous version of the Rayleigh-Taylor instability, we assume a zero velocity baseflow and two fluids separated by a common interface. We analyze the evolution of the perturbations on the baseflow assumed. In particular, we are interested in the development of two-dimensional flow structures and the growth rates of the different unstable modes. The calculations have been performed either in 1D or 2D computational domains, validating in both cases the inviscid hypothesis. For the 1D geometry, the equations have been formulated as a system of three,

two, and one equations depending on the number of fluid variables eliminated by algebraic manipulations. Depending on the number of equations used, the order of the system of differential equations could change; consequently, the boundary conditions must be reformulated accordingly.

Let ρ_1, μ_1, ν_1 and ρ_2, μ_2, ν_2 denote the densities and kinematic and dynamic viscosities of the top (heavy) and bottom (light) fluids, respectively. The two phase flow is governed by the incompressible Newtonian Navier-Stokes equations in a domain Ω. The domain will be a rectangle of height $2H$ and width $2L$ contained on the XY plane, mathematically expressed as $\Omega = [-L, L]x[-H, H]$. The nondimensional version of this set of equations reads:

$$\rho \frac{\partial \boldsymbol{u}}{\partial t} + \rho \boldsymbol{u} \cdot \nabla \boldsymbol{u} = -\nabla p + \rho \boldsymbol{u}_g + \nabla[\mu(\nabla \boldsymbol{u} + \nabla \boldsymbol{u}^T)], \quad (1a)$$

$$\nabla \cdot \boldsymbol{u} = 0, \quad (1b)$$

$$\frac{\partial \rho}{\partial t} + \boldsymbol{u} \cdot \nabla \rho = 0, \quad (1c)$$

where ρ, $\boldsymbol{u}$, p, t, ∇, μ, and $\boldsymbol{u}_g$ are the nondimensional density, velocity, pressure, time, nabla operator, viscosity, and unity vector representing gravity.

Similarly to Ref. [14], the characteristic time, length, velocity, pressure, density, and viscosity scales are defined as:

$$\rho_o = \frac{\rho_1 + \rho_2}{2}, \ \ \mu_o = \frac{\mu_1 + \mu_2}{2}, \ \ \nu_o = \frac{\nu_1 + \nu_2}{2}, \quad (2)$$

$$t_o = (\nu_0/g^2)^{1/3}, \ \ l_o = (\nu_0^2/g)^{1/3}, \ \ u_o = (g\nu_0)^{1/3}, \quad (3)$$

$$k_o = (\nu_0^2/g)^{-1/3}, \ \ p_o = \rho_0 g(\nu_0^2/g)^{1/3}. \quad (4)$$

A steady nonparallel basic flow $(\overline{u}_i, \overline{\rho}, \overline{p})$ is perturbed by small-amplitude velocity $\widetilde{u}_i$, density $\widetilde{\rho}$, and pressure $\widetilde{p}$ perturbations as follows:

$$u_i(x, y, z, t) = \overline{u}_i(x, y) + \varepsilon \widetilde{u}_i(x, y, z, t) + \text{c.c.}, \quad (5)$$

$$p(x, y, z, t) = \overline{p}(x, y) + \varepsilon \widetilde{p}(x, y, z, t) + \text{c.c.}, \quad (6)$$

$$\rho(x, y, z, t) = \overline{\rho}(x, y) + \varepsilon \widetilde{\rho}(x, y, z, t) + \text{c.c.}, \quad (7)$$

where $\varepsilon \ll 1$ and c.c. denotes the conjugate of the complex quantities $\widetilde{u}_i$, $\widetilde{\rho}$, and $\widetilde{p}$. As baseflow, we consider two superposed fluids and static fluids $\overline{u}_i = 0$ separated by a diffuse interface centered about $y = 0$ and subjected to a constant gravitational acceleration in the vertical direction y.

Therefore, in order to describe the Rayleigh-Taylor (RT) instability of sharp interface, it seems more consistent to attempt to solve the problem for a transition layer of finite thickness and then take the limit when the thickness tends to zero. In order to examine the sharp jump limit, we adopt the density and viscosity profiles

$$\overline{\rho} = 1 + A_\rho \tanh(y/L_s) \qquad \mu = 1 + A_\mu \tanh(y/L_s), \quad (8)$$

where L_s is the gradient scale length of the density and viscosity layers and A_ρ, A_μ the Atwood numbers given by

$$A_\rho = \frac{\rho_1 - \rho_2}{\rho_1 + \rho_2} \qquad A_\mu = \frac{\mu_1 - \mu_2}{\mu_1 + \mu_2}. \quad (9)$$

Taking account of Eqs. (8), typical air-water hydrodynamic instabilities in the presence of a sharp interface can be

recovered by setting $L_s \to 0$. When Eqs. (5), (6), and (7) are substituted into the Navier-Stokes equations (1a), (1b), and (1c), assuming zero basic flow $\overline{u}_i = 0$ and neglecting second-order terms, the linearized Navier-Stokes equations for the perturbation quantities are obtained:

$$\overline{\rho} \frac{\partial \widetilde{u}_i}{\partial t} = -\frac{\partial \widetilde{p}}{\partial x_i} + \mu \Delta \hat{u}_i + \left(\frac{\partial \widetilde{u}_j}{\partial x_i} + \frac{\partial \widetilde{u}_i}{\partial x_j} \right) \frac{\partial \mu}{\partial x_j} + \widetilde{\rho} u_{g_i}, \quad (10)$$

$$\frac{\partial \widetilde{\rho}}{\partial t} + \widetilde{u}_j \frac{\partial \overline{\rho}}{\partial x_j} = 0, \quad (11)$$

$$\frac{\partial \widetilde{u}_i}{\partial x_i} = 0. \quad (12)$$

Since the coefficients of $\widetilde{u}_i$, $\widetilde{\rho}$, and $\widetilde{p}$ do not depend on z and t the perturbations quantities can be written as normal modes,

$$\tilde{u}_i(x, y, z, t) = \hat{u}_i(x, y)e^{k_z z}e^{\gamma t} + \text{c.c.}, \quad (13a)$$

$$\tilde{p}(x, y, z, t) = \hat{p}(x, y)e^{k_z z}e^{\gamma t} + \text{c.c.}, \quad (13b)$$

$$\tilde{\rho}(x, y, z, t) = \hat{\rho}(x, y)e^{k_z z}e^{\gamma t} + \text{c.c.}, \quad (13c)$$

where the complex conjugate is required to render the perturbations real. Additionally, $\gamma = \sigma + i\omega \in \mathbb{C}$ is the complex growth or decay rate σ and oscillation frequency ω.

In the following, two different numerical methods will be used depending on the hypothesis used to solve the linearized Navier-Stokes equations around a baseflow. The first formulation uses a Chebyshev collocation method [15] when the geometry is simplified to 1D, and the second performs a 2D variational formulation of the equations using a second-order finite element discretization based on the Galerkin method [16].

III. MATHEMATICAL MODELS

A. Linear stability: Two-dimensional eigenvalue-problem formulation and solution methodology

We are interested in the temporal stability analysis on a 2D computational domain ($k_z = 0$) with homogeneous Dirichlet boundary conditions on the top and bottom boundaries and periodic boundary conditions between the right and left boundaries. Consequently, this framework does not contain any explicit z coordinate. A 3D generalization of this framework, where the perturbations assume a spanwise periodic length (i.e., homogeneous direction) and L_z is defined through the real wave number $k_z = \frac{2\pi}{L_z} \in \mathbb{R}$, can be obtained in [16].

The resulting system is solved in a 2D $(x, y) \in [-L, L]x[-H, H]$ computational domain. In this case, a periodic boundary condition is imposed between the boundaries placed at $x = \pm L$, see Fig. 1. This is a relevant difference when compared to the classic 1D instability analysis of the RTI which assumes periodic solution in both the horizontal x and spanwise z directions [12]. Here the BiGlobal EVP [17] [Eqs. (10)–(12)] has been solved without the need to resort to the periodic assumption in the horizontal x direction and infinite spanwise length. The perturbation flow must satisfy the no-slip boundary conditions $\tilde{u} = 0$ on $y = \pm H$.
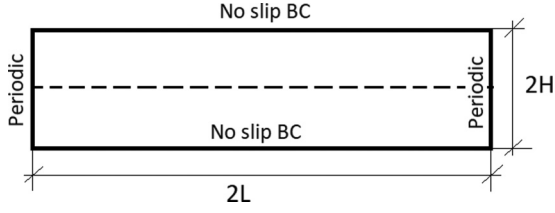
FIG. 1. Scheme of the geometry used for the 2D viscous simulation. A dashed line indicates the $y = 0$ coordinate. The boundary conditions are also written at each boundary.

For the present case, where the baseflow velocity is zero, we have a real eigenvalue problem where the third equation (14c), which contain the velocity perturbation component $\hat{w}$, can be decoupled from the rest. Substitution of the ansatz (13) into the perturbation equations (10) and (11) yields

$$\mathcal{L}\hat{u} + \frac{\partial \hat{p}}{\partial x} - \frac{d\mu}{dy}\left(\frac{\partial \hat{v}}{\partial x} + \frac{\partial \hat{u}}{\partial y}\right) = -\gamma\overline{\rho}\hat{u}, \qquad (14a)$$

$$\mathcal{L}\hat{v} + \frac{\partial \hat{p}}{\partial y} - 2\frac{d\mu}{dy}\frac{\partial \hat{v}}{\partial y} + \hat{\rho} = -\gamma\overline{\rho}\hat{v}, \qquad (14b)$$

$$\mathcal{L}\hat{w} - \frac{d\mu}{dy}\left(\frac{\partial \hat{w}}{\partial y}\right) = -\gamma\overline{\rho}\hat{w}, \qquad (14c)$$

$$\frac{\partial \hat{u}}{\partial x} + \frac{\partial \hat{v}}{\partial y} = 0, \qquad (14d)$$

$$\hat{v}\frac{d\rho}{dy} = -\gamma\hat{\rho}, \qquad (14e)$$

where $\mathcal{L}$ is the linear advection-diffusion operator:

$$\mathcal{L} = -\mu\left(\frac{\partial^2}{\partial x^2} + \frac{\partial^2}{\partial y^2}\right). \qquad (15)$$

This converts system (14) into a real generalized eigenvalue problem:

$$A \cdot X = -\gamma B \cdot X, \qquad (16)$$

where X $= (\hat{u}, \hat{v}, \hat{w}, \hat{\rho}, \hat{p})^{\mathrm{T}}$ with real linear operators A and B. The boundary conditions for this problem are

$$\hat{u}(-L, y) = \hat{u}(L, y), \qquad (17)$$

$$\hat{v}(-L, y) = \hat{v}(L, y), \qquad (18)$$

$$\hat{u}(x, \pm H) = 0, \qquad (19)$$

$$\hat{v}(x, \pm H) = 0. \qquad (20)$$

The eigenvalues γ of such a real eigenvalue problem are either real or they arise as pairs of complex conjugate eigenvalues. Adopting the existing nomenclature from the literature, see, e.g.. Theofilis *et al.* [18], the corresponding eigenvectors describe either stationary modes ($\gamma = 0$) or traveling waves ($\gamma = \pm i\omega \neq 0$).

To discretize the equations, we use a triangular-element-based unstructured mesh. The eigenvalue problem is solved using a Krylov-subspace iteration, originally proposed in Ref. [19] and discussed in detail in Ref. [17]. In order to check the accuracy of the results during the stability analysis,

the number of mesh nodes is increased until three significant digits of the most unstable eigenvalue were converged.

B. Linear stability: One-dimensional eigenvalue-problem formulation and solution methodology

System (10)–(12) is now simplified using the assumptions

$$\tilde{u}_i(x, y, z) = \hat{u}_i(y)\exp(ik_x x)\exp(ik_z z), \qquad (21)$$

$$\tilde{\rho}(x, y, z) = \hat{\rho}(y)\exp(ik_x x)\exp(ik_z z), \qquad (22)$$

$$\tilde{p}(x, y, z) = \hat{p}(y)\exp(ik_x x)\exp(ik_z z), \qquad (23)$$

where N discrete points were used in the 1D computational domain $y \in [-H, H]$.

Consequently, using the ansatz given by (21)–(23), Eqs. (14a)–(14e) can be written as

$$ik_x\hat{p} - \mu(D^2 - k^2)\hat{u} - D\mu(ik_x\hat{v} + D\hat{u}) = -\gamma\overline{\rho}\hat{u}, \qquad (24)$$

$$D\hat{p} - \mu(D^2 - k^2)\hat{v} - 2D\mu D\hat{v} + \hat{\rho} = -\gamma\overline{\rho}\hat{v}, \qquad (25)$$

$$-k_z\hat{p} - \mu(D^2 - k^2)\hat{w} - D\mu(-k_z\hat{v} + D\hat{w}) = -\gamma\overline{\rho}\hat{w}, \qquad (26)$$

$$D\overline{\rho}\hat{v} = -\gamma\hat{\rho}, \qquad (27)$$

$$ik_x\hat{u} + k_z\hat{w} = -D\hat{v}, \qquad (28)$$

where $k^2 = k_x^2 + k_z^2$ and $D = d/dy$. In this velocity-pressure-density formulation only homogeneous Dirichlet boundary conditions for all components of the velocity perturbation at $y = \pm H$ are imposed. Now the complex generalized eigenvalue problem for the determination of γ may thus be written as

$$A\begin{pmatrix}\hat{u}\\\hat{v}\\\hat{w}\\\hat{\rho}\\\hat{p}\end{pmatrix} = -\gamma B\begin{pmatrix}\hat{u}\\\hat{v}\\\hat{w}\\\hat{\rho}\\\hat{p}\end{pmatrix}, \qquad (29)$$

where the matrix A can be expressed as

$$A = \begin{pmatrix} L & -D\mu ik_x & 0 & 0 & ik_x \\ 0 & L - D\mu D & 0 & 1 & D \\ 0 & k_z D\mu & L & 0 & -k_z \\ 0 & D\hat{\rho} & 0 & 0 & 0 \\ ik_x & D & k_z & 0 & 0 \end{pmatrix} \qquad (30)$$

with the operator L,

$$L = -\mu(D^2 - k^2) - D\mu D, \qquad (31)$$

where the matrix B

$$B = \begin{pmatrix} \overline{\rho} & 0 & 0 & 0 & 0 \\ 0 & \overline{\rho} & 0 & 0 & 0 \\ 0 & 0 & \overline{\rho} & 0 & 0 \\ 0 & 0 & 0 & 1 & 0 \\ 0 & 0 & 0 & 0 & 0 \end{pmatrix}. \qquad (32)$$

Now, multiplying Eq. (24) by ik_x and Eq. (26) by k_z, and making use of Eq. (28), we eliminate components $\hat{u}$ and $\hat{w}$ of

the perturbation velocity and obtain

$$k^2\hat{p} = [-\gamma\overline{\rho} + \mu(D^2 - k^2)]D\hat{v} + (D\mu)(D^2 + k^2)\hat{v}. \quad (33)$$

Using Eqs. (25), (27), and (33), we obtain a reduced third-order generalized eigenvalue problem system where the eigenvectors are formed by the vertical velocity, density, and pressure perturbations,

$$A\begin{pmatrix}\hat{v}\\\hat{p}\\\hat{\rho}\end{pmatrix} = \gamma B\begin{pmatrix}\hat{v}\\\hat{p}\\\hat{\rho}\end{pmatrix}. \quad (34)$$

In this vertical velocity-density-pressure formulation, homogeneous Dirichlet boundary conditions are applied for the vertical velocity and the normal derivative of the vertical velocity perturbations.

$$\hat{v}(y = \pm H) = 0, \quad D\hat{v}(y = \pm H) = 0, \quad (35)$$

with the A and B operators

$$A = \begin{bmatrix} \mu(D^2 - k^2) + 2D\mu D & -D & -I \\ \mu(D^3 - k^2 D) + D\mu(D^2 + k^2) & -k^2 & 0 \\ -D\overline{\rho} & 0 & 0 \end{bmatrix} \quad (36)$$

and

$$B = \begin{pmatrix} \overline{\rho} & 0 & 0 \\ \overline{\rho}D & 0 & 0 \\ 0 & 0 & I \end{pmatrix}, \quad (37)$$

where I is the identity matrix. This system can be reduced to only one dimensionless stability equation for the vertical velocity perturbation $\hat{v}$:

$$A\gamma^2 + B\gamma + C = 0, \quad (38)$$

where A, B, and C are, respectively,

$$A = k^2\overline{\rho}\hat{v} - D\overline{\rho}D\hat{v} - \overline{\rho}D^2\hat{v}, \quad (39)$$

$$B = \mu(D^4 + k^4 - 2k^2D^2)\hat{v} + 2(D\mu)(D^3 - k^2D)\hat{v}, \quad (40)$$
$$+ (D^2\mu)(D^2 + k^2)\hat{v}$$

$$C = -k^2 D\overline{\rho}\hat{v}. \quad (41)$$

Equation (38) in conjunction with the boundary conditions

$$\hat{v}(y = \pm H) = 0 \quad D\hat{v}(y = \pm H) = 0 \quad (42)$$

constitutes the quadratic eigenvalue problem for γ. This is the same fourth-order ODE presented in Ref. [14] for two separated constant density and viscosity fluids, solved in Ref. [8], when boundary conditions are imposed at the interface that link both regions.

IV. RESULTS

For a given wave number k, the viscous eigenvalue problems given by expressions (38)–(42) (in 1D) and (16) and (17) (in 2D) are numerically solved using the respective boundary conditions, which gives the eigenvalues and the corresponding eigenfunctions. A spectral Chebyshev collocation and a
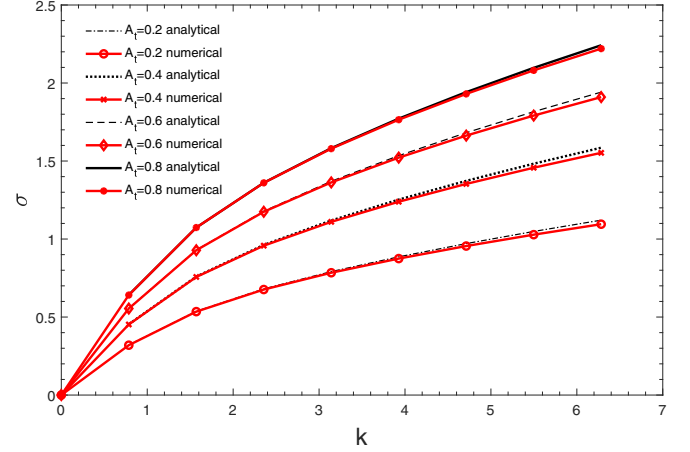

FIG. 2. Growth rate σ of the most unstable eigenvalue in the inviscid case versus the wave number k for different values of the Atwood number $A_\rho = 0.2, 0.4, 0.6, 0.8$ for $H = 1$ and $L_s = 0.01$. The expression (43) is added in black lines for comparison.

finite element scheme are used for the 1D and 2D domains, respectively.

A. Validation: Inviscid 1D problem

As a previous validation the inviscid limit $\mu = D\mu = 0$ is studied. The analytical result that corresponds to the dimensionless classical RTI growth rate, see Ref. [9], is given by the following expression:

$$\gamma_C = \sigma = \sqrt{A_\rho k \tanh(kH)}. \quad (43)$$

A full spectrum is obtained when the inviscid version of eigenvalue problem 38 is numerically solved. Except the maximum eigenvalue which is widely investigated and approximates the classical value γ_C, we also find many other eigenmodes with smaller eigenvalues. The smaller eigenvalues in the study of RTI have so far not been paid enough attention by researchers.
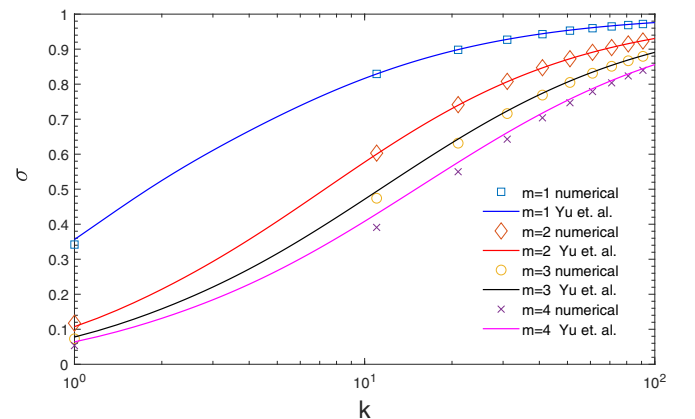

FIG. 3. Growth rate σ of the most unstable and three less stable internal modes versus the wave number k for $A_\rho = 0.2$, $L_s = 0.203$, and $H = 1$. The results from the analytic expression (44) when $H = 1$ have been added for comparison.
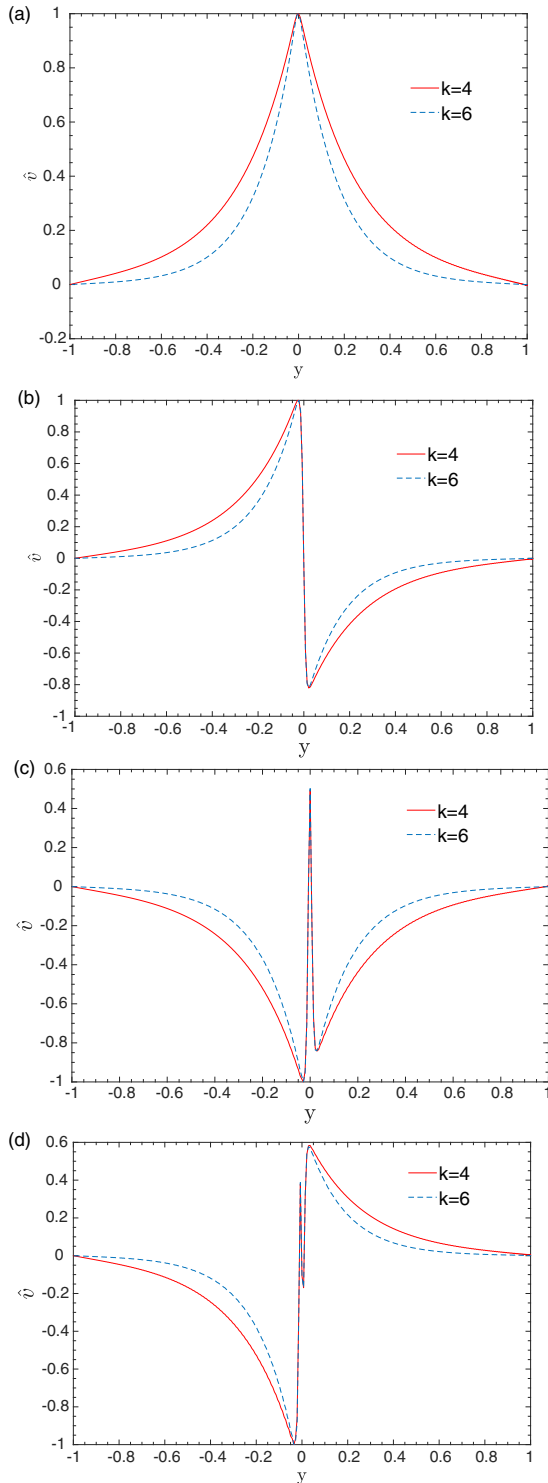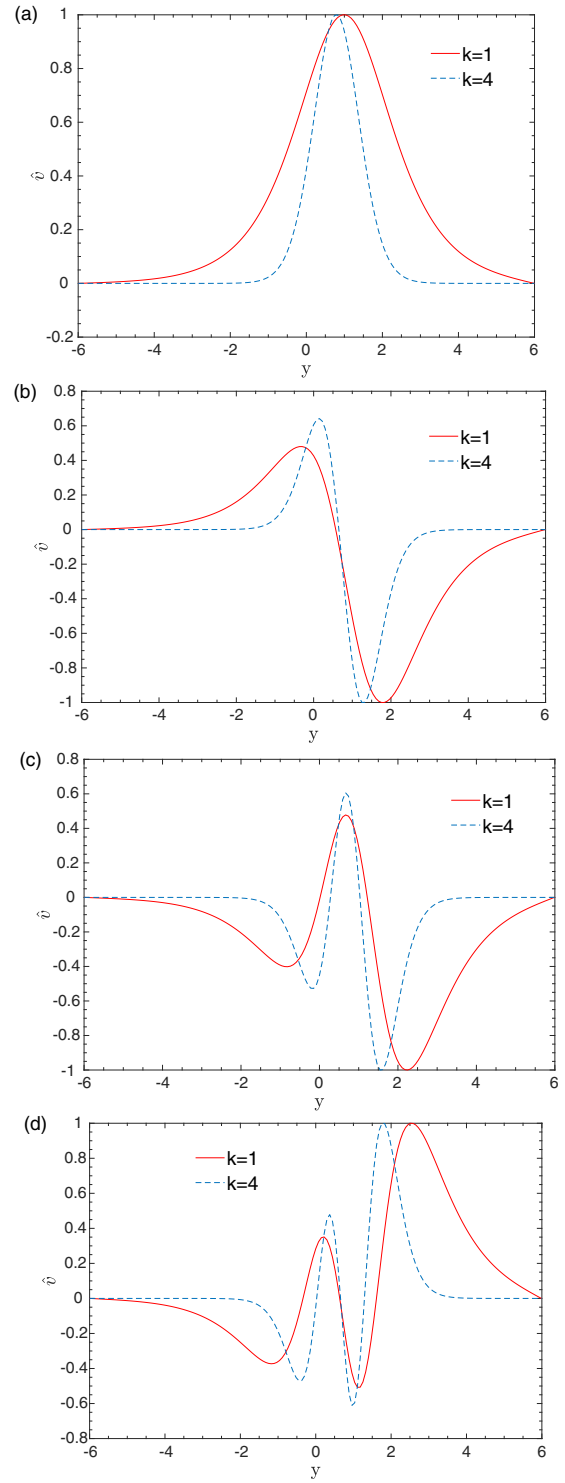
FIG. 4. Eigenvectors of the vertical velocity component $\tilde{v}$ corresponding to the four most unstable modes $m = 1$ (a), $m = 2$ (b), $m = 3$ (c), and $m = 4$ (d) for the wave numbers $k = 4$ and $k = 6$ for $A_\rho = 0.2$. Other parameters are $L_s = 0.01$ and $H = 1$.

FIG. 5. Eigenvectors of the vertical velocity component $\tilde{v}$ corresponding to the four most unstable modes $m = 1$ (a), $m = 2$ (b), $m = 3$ (c), and $m = 4$ (d) for the wave numbers $k = 1$ and $k = 4$ for $A_\rho = 0.8$. Other parameters are $L_s = 0.203$ and $H = 6$.

Figure 2 shows the linear growth rates of the leading mode as a function of the normalized wave number for different Atwood numbers. The numerical results are obtained for a low value of the density gradient scale length $L_s = 0.01$, which corresponds to a steep transition between both fluids. The

numerical eigenvalues are compared to the analytic results from [8] for $N = 256$ Gauss-Lobatto points, obtaining an accurate matching.

For smoothly varying density interfaces, Fig. 3 shows the linear growth rates of the four less unstable modes as a
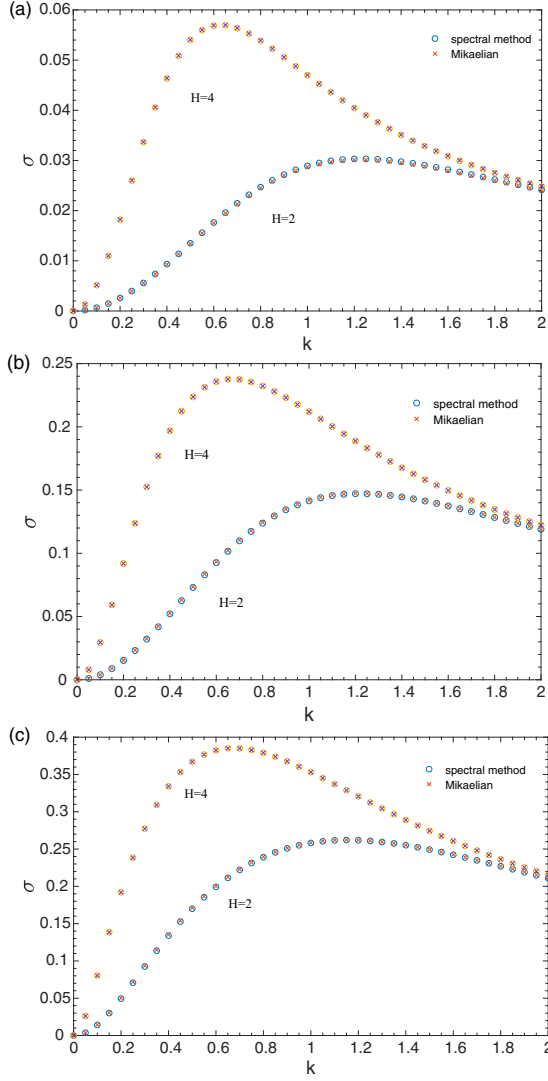
FIG. 6. Dependence of the growth rate σ on k for $A_\rho = A_\mu = 0.1$ (a), $A_\rho = A_\mu = 0.5$ (b), and $A_\rho = A_\mu = 0.9$ (c). The upper and the lower curves correspond to $H = 4$ and $H = 2$, respectively. Previous numerical calculations [8] and spectral method ($L_s = 0.01$ and $N = 256$) are plotted.

function of the normalized wave number k for the Atwood number $A_\rho = 0.2$ and $L_s = 0.203$. For comparison, an extended version for finite H values of the expression (5) or Ref. [35] in Ref. [12] for $A_\rho < 0.6$ and $H \to \infty$ is obtained as:

$$\gamma_m = \sqrt{\frac{A_\rho^2 k^2 \tanh(kH)}{(1 + A_\rho k)[2(m-1) + A_\rho k]}} \quad m = 1, 2, 3, \ldots,$$
(44)

Results are compared in Fig. 3 and all modes agree very well with the values γ_m, obtained from corrected expression (44) for finite domains of length $2H$. As expected for all these modes, the linear growth rates increase with the wave number and approach unity as the wave number tends to infinity. The first mode ($m = 1$) has the maximal growth rate and agrees well with the classical value of γ_C, which is represented in Fig. 3 by a continuous blue line.
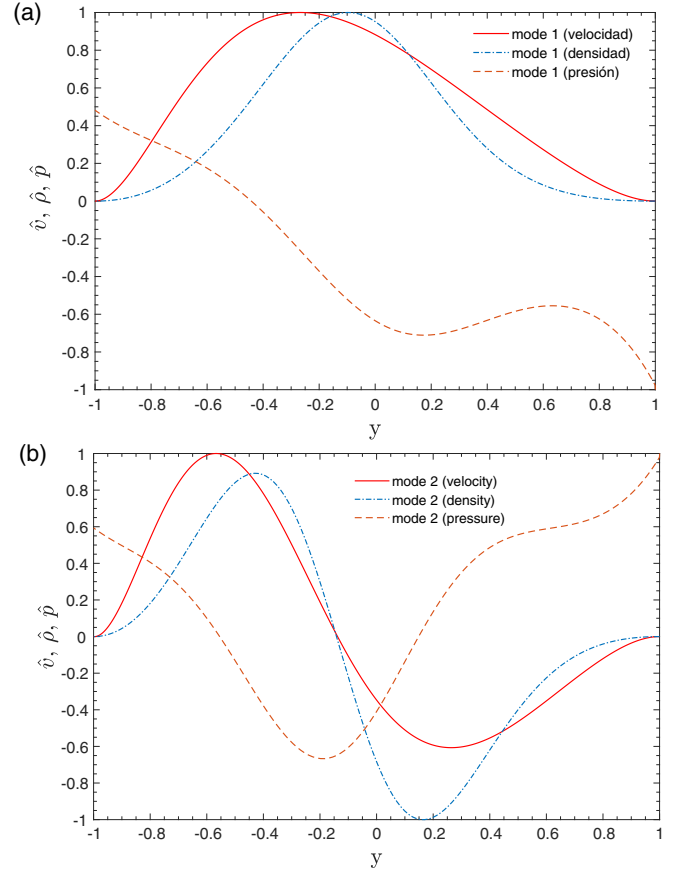

FIG. 7. Two most unstable vertical velocity, density and pressure eigenvectors $m = 1$ (a) and $m = 2$ (b) for the 1D domain in the viscous case, where $k = \pi$ $A_\rho = A_\mu = 0.9$, $L_s = 0.5$, and $H = 1$.

Figures 4 and 5 show the vertical velocity eigenfunctions $\tilde{v}$ corresponding to the four least stable modes for the wave numbers $k = 4$ and $k = 6$ when the Atwood number is $A_\rho = 0.2$ and $L_s = 0.01$ and $k = 1$ and $k = 4$ for an Atwood number of $A_\rho = 0.8$ and $L_s = 0.203$. The first case represents two similar density fluids with a sharp interface and the second two fluids with a significant density difference and a smooth transition between them. As can be observed, higher modes present more complex structures, especially on the interface area. As with what happens in similar studies, see Ref. [12], the number of local maxima and minima are related to the order of the eigenmode. This means that the first eigenmode contains one local maximum, the second contains one maximum and one minimum, the third two minimums and one maximum, etc.

B. Viscous problem

1. Viscous 1D problem

Figure 6 shows the numerical results obtained when viscous problem (38) is solved using a sharp interface with density and viscosity gradient scale length $L_s = 0.01$. The results are compared to the results in Ref. [8] using two different phases and boundary conditions in the interface between them. The calculations have been performed for $A_\rho = A_\mu = 0.1, 0.5, 0.9$ using two different computational domains of
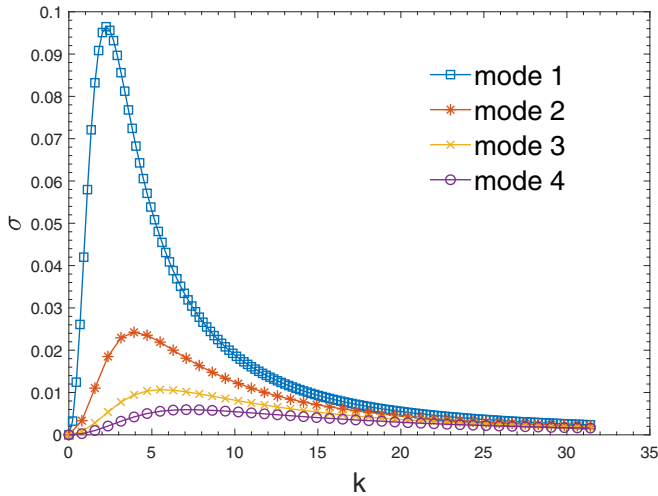
FIG. 8. Dependence of the viscous growth rate σ on k for $A_\rho = A_\mu = 0.9$, $L_s = 0.5$, and $H = 1$ for the four least unstable modes $m = 1, 2, 3, 4$.

height $H = 2$ and $H = 4$. The comparisons present very good agreement. As expected, and differing from the inviscid case, in the viscous case the curves do not present a monotonic growing tendency, and a maximum is always found.

Figure 7 shows the two most unstable modes corresponding to the fluid variables, vertical velocity, density, and pressure, when the problem is solved for $k = 1$ in 1D with $A_\rho = A_\mu = 0.9$, density and viscosity gradient scale length $L_s = 0.5$, and computational size $H = 1$. In this work, apart from the vertical velocity eigenmodes normally presented in the literature, the density and pressure structures of the eigenvectors are also shown. The density follows the tendency of the velocity, verifying that the number of maxima and minima correspond to the order of the eigenmode, but the pressure does not follow that rule.

Figure 8 shows the growth rate of the four most unstable values when $A_\rho = A_\mu = 0.9$, $L_s = 0.5$, and $H = 1$, when the computation is performed in 1D. The shape of the distribution follows for all modes the typical shape also found for the most unstable one in Fig. 6, where in all cases a local maximum is always found.

2. Viscous 2D problem

Now the computation turns to 2D, where the computational domain is defined by a rectangle of $2L$ by $2H$ and the discretization is performed by finite elements, using Taylor-Hood triangular elements [16]. The density perturbation was approximated by second-order polynomials. All the computations are performed in a computational domain $H = 1$ and
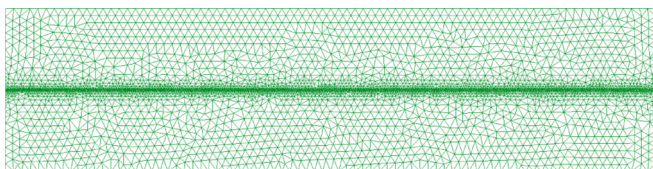

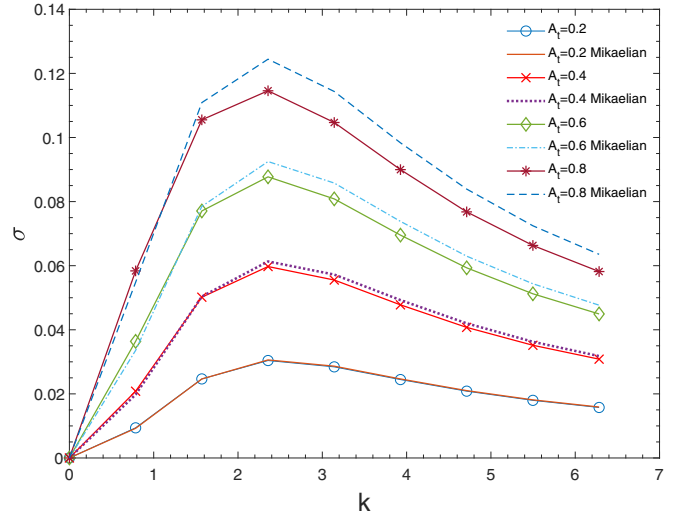FIG. 9. Mesh used for the 2D viscous simulation.

FIG. 10. Dependence of the viscous growth rate σ on k for $A_\rho = A_\mu = 0.8, 0.6, 0.4, 0.2$ and $H = 1$. Referenced numerical calculations [8] and FEM in 2D ($L_s = 0.01$) are plotted.

$L = 4$. The number of quadratic mesh nodes and triangular elements is 23 145 and 11 458, respectively, where the mesh has been refined around the horizontal line $y = 0$, see Fig. 9.

It should be noted that the numerical accuracy of this second-order method in this case is lower than the one obtained by the 1D spectral Chebyshev, but it allows more complex computations in the future that cannot be performed in 1D, such as complex baseflows involved in the instability onset. In Fig. 10, the growth rate dependance on
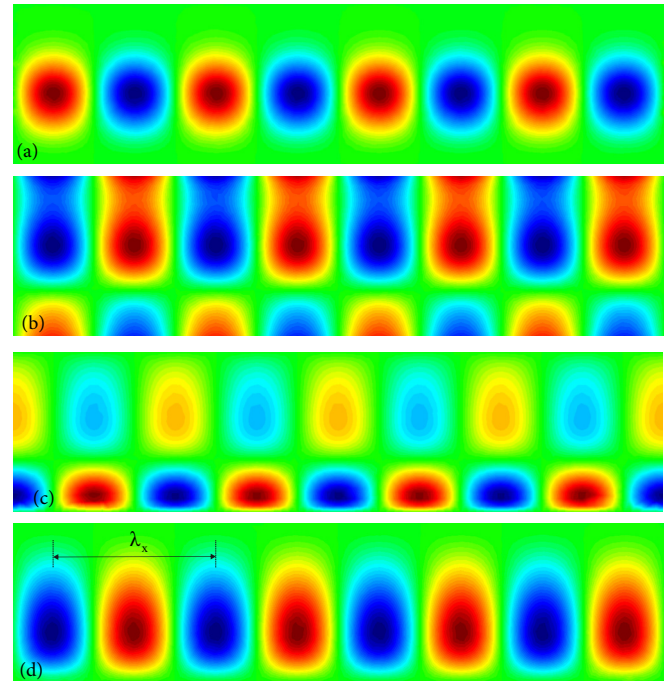

FIG. 11. Most unstable perturbation for the case $k_x = \pi$, $H = 1$, $L = 4$, and $A_\mu = A_\rho = 0.9$. (a) Density, (b) pressure, (c) horizontal velocity, and (d) vertical velocity. The computation was performed with the interface parameter $L_s = 0.5$.
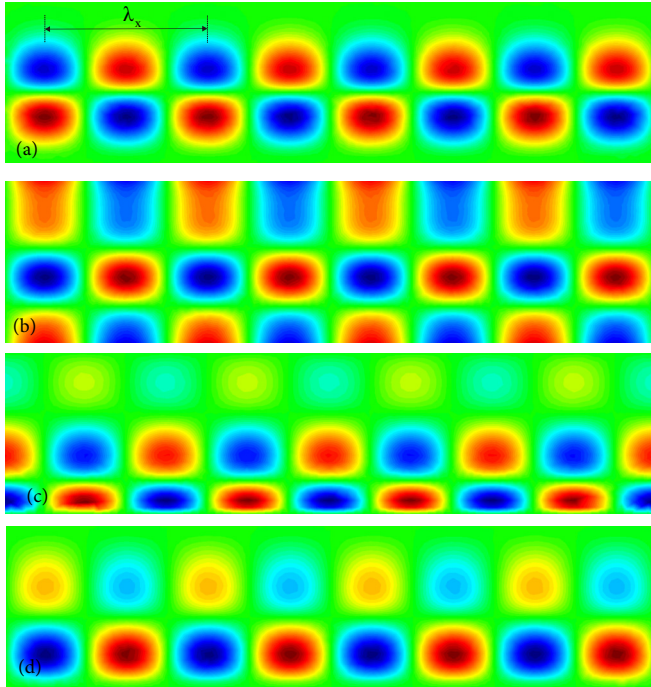
FIG. 12. Second-most unstable perturbation for the case $k_x = \pi$, $H = 1$, and $A_\mu = A_\rho = 0.9$. (a) Density, (b) pressure, (c) horizontal velocity, and (d) vertical velocity. The computation was performed with the interface parameter $L_s = 0.5$.

the wave number for the most unstable mode is computed for several equal viscosity and density ratios $A_\rho = A_\mu = 0.8, 0.6, 0.4, 0.2$ when the density and viscosity gradient scale length is $L_s = 0.01$. Again, all ratios present a local maximum that increases with the Atwood number. It can be observed that the higher the Atwood number, the larger the difference between the computed value in 2D and the reference value obtained by spectral methods in the 1D case. However, the 2D computation allows the possibility of studying more complex geometries than the ones normally studied in the RTI.

In Fig. 11, the most unstable perturbation for all the fluid variables is represented for a large density gradient scale length $L_s = 0.5$ and $k_x = \pi$. The periodic structure is clearly appreciated and the wave length is $\lambda_x = 2\pi / k_x = 2$ which can be also confirmed in the figure.

In Fig. 12, the second most unstable perturbation is also represented for $L_s = 0.5$ and $k_x = \pi$. As expected, the structure of the second mode ($m = 2$) is more complex, and the number of maxima or minima in the components of the vertical velocity perturbation and density increase with m.

V. CONCLUSIONS

In this work, a complete numerical description of the RTI in both the viscous and the inviscid case has been addressed using a single domain where the fluid properties vary according to a hyperbolic tangent function. This viscous formulation has been used in 1D and 2D, and it is able to describe the RTI without implementing any boundary condition for the interface. As result, the RTI is able to produce a spectrum of multiple eigenvalues and the corresponding eigenvectors. The spectrum is formed by a leading eigenvalue, well studied in previous literature, but the rest of the spectrum has not been so extensively studied, especially in the viscous case.

The fitting expression proposed in the literature [12] for the inviscid case was generalized for a finite domain and used as a reference for validation. Our numerical 1D formulation with a single fluid of variable density and viscosity was compared for viscous cases with the results provided in Ref. [8] obtaining a very good agreement for a wide range of density and viscosity ratios. The results are computed both in a 1D computational domain using a spectral discretization and then also generalized to a 2D domain where a typical FEM discretization is used.

The possibilities contained within the 2D formulation allow us to include more complex geometries and baseflows than the ones used for the classical RTI. The formulation presented here allows the presence of submerged objects or previously computed biphasic solutions of the Navier-Stokes equations.

The present work also generalizes the potential applications of fluid mixing that appear in many areas to those cases where viscosity has a relevant role. The paper quantifies how viscosity affects higher modes which have have relatively smaller linear growth rates. Future applications will be performed in the near future, where the RTI is studied inside nonrectangular shapes.

[1] L. Rayleigh, Proc. Lond. Math. Soc. **s1-14**, 170 (1882); G. I. Taylor, Proc. R. Soc. Lond. **A 201**, 1921 (1950).

[2] R. E. Rosensweig, Y. Hirota, S. Tsuda, and K. Raj, J. Phys.: Condens. Matter **20**, 204147 (2008).

[3] C. Harig, P. Molnar, and G. A. Houseman, Tectonics **27**, TC6019 (2008).

[4] T. M. Willey, K. Champley, R. Hodgin, L. Lauderbach, M. Bagge-Hansen, C. May, N. Sanchez, B. J. Jensen, A. Iverson, and T. van Buuren, J. Appl. Phys. **119**, 235901 (2016).

[5] T. G. Theofanous, Annu. Rev. Fluid Mech. **43**, 661 (2011).

[6] A. A. Blinova, M. M. Romanova, and R. V. E. Lovelace, Mon. Not. R. Astron. Soc. **459**, 2354 (2016).

[7] L. H. A. Tavakoli and D. D. Tskhakayab, Phys. Plasmas **7**, 89 (1999).

[8] K. O. Mikaelian, Phys. Rev. E **54**, 3676 (1996).

[9] M. H. O. Allah, Indian J. Pure Appl. Math. **32**, 303 (2001).

[10] R. V. Morgan, O. A. Likhachev, and J. W. Jacobs, J. Fluid Mech. **791**, 34 (2016).

[11] R. Duff, F. H. Harlow, and C. W. Hirt, Phys. Fluids **5**, 417 (1962).

[12] C. X. Yu, C. Xue, J. Liu, X. Y. Hu, Y. Y. Liu, W. H. Ye, L. F. Wang, J. F. Wu, and Z. F. Fan, Phys. Rev. E **97**, 013102 (2018).

[13] M. Dong, Z. Fan, and C. Yu, Phys. Rev. E **99**, 013109 (2019).

[14] S. Chandrasekhar, *Hydrodynamic and Hydromagnetic Stability* (Dover, New-York, 1981).

[15] C. Canuto, M. Y. Hussaini, A. Quarteroni, and T. A. Zang, *Spectral Methods: Fundamentals in Single Domains* (Springer, New York, 2006).

[16] L. González, V. Theofilis, and R. Gómez-Blanco, AIAA J. **45**, 840 (2007).

[17] V. Theofilis, Prog. Aero. Sci. **39**, 249 (2003).

[18] V. Theofilis, P. W. Duck, and J. Owen, J. Fluid. Mech. **505**, 249 (2004).

[19] Y. Saad, Lin. Algebra. Appl. **34**, 269 (1980).

Correction: A second affiliation indicator was inserted for the second author.